

Magnetic domain walls in constrained geometries

P.-O. Jubert,* R. Allenspach, and A. Bischof

IBM Research, Zurich Research Laboratory, CH-8803 Rüschlikon, Switzerland

Magnetic domain walls have been studied in micrometer-sized $\text{Fe}_{20}\text{Ni}_{80}$ elements containing geometrical constrictions by spin-polarized scanning electron microscopy and numerical simulations. By controlling the constriction dimensions, the wall width can be tailored and the wall type modified. In particular, the width of a 180° Néel wall can be strongly reduced or increased by the constriction geometry compared with the wall in unconstrained systems.

PACS numbers: 75.60.Ch, 75.75.+a, 75.70.Kw

For almost a century, the width of magnetic domain walls (DWs) has been believed to be determined by material properties only. However, recent investigations on DWs in nanometer-scale systems have revealed new physical properties due to the geometrical confinement of the magnetization. A reduction of the Bloch wall width has been predicted¹ and observed² in nanometer-sized constrictions. This effect is thought to be the origin of the large magneto-resistance measured in nanocontacts, and explained by ballistic transport through a narrow DW pinned within the contact.^{3,4,5} Furthermore, domain walls are now being investigated as tiny individual magnetic objects that can be manipulated in view of their potential for application in novel magnetic logic or memory devices.⁶ Of interest in this field are the possibilities of pinning DWs at constrictions and of displacing them using a magnetic field⁷ or an applied current.^{8,9,10,11,12} For all these phenomena, the key parameter is the magnetic structure of the domain walls. For a basic understanding as well as for potential applications, it is important to gain quantitative insight into how DW properties can be modified via the geometry.

The prediction of DW narrowing in a constriction was based on a ferromagnetic model system containing a planar Bloch wall.¹ Because dipolar contributions in the constriction were neglected, the problem was one-dimensional and could be solved analytically. The vast majority of small elements, however, exhibits DWs of Néel type, with a nonvanishing magnetization component perpendicular to the wall. In these walls, the dipolar energy determines the wall profile to a large extent, and hence the problem is more intricate.

In this paper, we investigate Néel-type walls in elements containing constrictions of controlled dimensions. The experimental results obtained by scanning electron microscopy with spin analysis (spin-SEM¹³ or SEMPA¹⁴) are compared with micromagnetic simulations. We demonstrate how the wall properties can be tuned both by the element size and the constriction dimensions. Constraining a DW in a micrometer-sized element strongly reduces the wall width compared with the width in an infinite film. By appropriately tuning the constriction dimensions, the Néel wall width can further be decreased, or alternatively, increased until the wall splits into two separate walls.

The constrictions were fabricated in thin, micrometer-sized rectangular elements by using electron-beam lithography and Ar dry etching of $\text{Fe}_{20}\text{Ni}_{80}$ thin films. These films were produced by sputter deposition on $\text{SiO}_2/\text{Si}(100)$, resulting in (111)-textured $\text{Fe}_{20}\text{Ni}_{80}$ films with a grain size of about 2 nm diameter, as determined from x-ray measurements. The crystalline anisotropy of the film was measured to be a superposition of a uniaxial term $K_u = 160 \text{ J/m}^3$ and a cubic term $K_1 = -150 \text{ J/m}^3$. The anisotropy is so low that it has no influence on the magnetic patterns in this study, as verified by micromagnetic simulations. All simulations were carried out using the OOMMF code.¹⁵ The material parameters used for the simulations are the commonly employed values for $\text{Fe}_{20}\text{Ni}_{80}$, an exchange constant $A_{\text{exch}} = 13 \times 10^{-12} \text{ J/m}$ and a saturation magnetization $M_s = 800 \text{ kA/m}$. The discretization cell size was 5 nm.

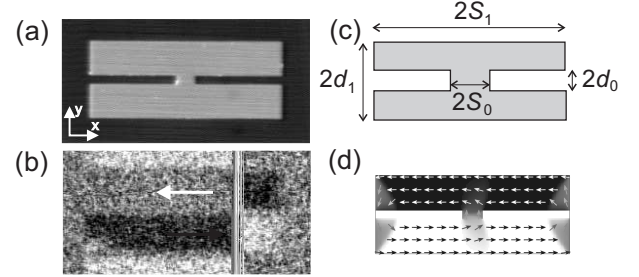


FIG. 1: (a) Topographic image of a $10 \mu\text{m} \times 4 \mu\text{m} \times 7.5 \text{ nm}$ $\text{Fe}_{20}\text{Ni}_{80}$ element with constriction dimensions $d_0 = 225 \text{ nm}$ and $S_0 = 500 \text{ nm}$. (b) Corresponding magnetic configuration after ac demagnetization as determined by spin-SEM. The arrows indicate the magnetization direction. (c) Schematic of the rectangular magnetic element with constriction. (d) Magnetic configuration calculated for an element having the same dimensions.

The magnetic configurations of the elements were investigated in our spin-SEM setup.¹⁶ Topography and magnetization distribution are determined simultaneously and with a lateral resolution of 20 to 30 nm. Thus, the technique is ideally suited for measuring DW profiles.^{17,18,19} The patterned sample was cleaned *in-situ* by gentle Ne sputtering to remove surface contaminants. Eventually, 1–2 monolayers of Fe were deposited *in-situ* onto the $\text{Fe}_{20}\text{Ni}_{80}$ sample. This enhances the electron spin polarization without affecting the magnetiza-

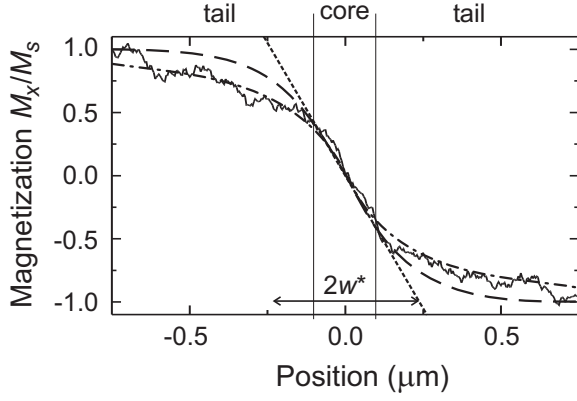


FIG. 2: Domain-wall profile measured for a $10 \mu\text{m} \times 4 \mu\text{m} \times 7.5 \text{ nm}$ $\text{Fe}_{20}\text{Ni}_{80}$ element with a constriction size of $d_0 = 225 \text{ nm}$ and $S_0 = 500 \text{ nm}$. The experimental profile is compared with the calculation (dash-dotted line) and an hyperbolic tangent function (dashed line). The profile is averaged over 80% of the constriction length $2S_0$.

tion configuration of the element.²⁰

The shape of the micrometer-sized elements has been chosen such as to facilitate the pinning of a 180° Néel wall inside the constriction. Because of the predominant magnetostatic contribution in $\text{Fe}_{20}\text{Ni}_{80}$, the lowest energy state is a two-domain configuration separated by a 180° Néel wall positioned in the constriction, see Fig. 1. This configuration is obtained experimentally after ac demagnetization. Without constriction, a single domain prevails. We restrict the film thickness to $\leq 20 \text{ nm}$ to ensure that the Néel walls are homogeneous throughout the element thickness.

The profile across the wall pinned in the constriction of Fig. 1 is shown in Fig. 2. Excellent agreement with the calculated profile is found. The typical features of a symmetrical Néel wall can be identified: The magnetization mainly rotates in the core of the wall, which can be approximated by a hyperbolic tangent function. In the outer regions, the profile shows a slower magnetization rotation and hence deviates from the tanh function. These long tails are typical for the Néel wall, and have been identified in thin films earlier.¹⁸ We quantify the wall by defining a mean DW width w^* , which is the inverse slope of the curve, fitted linearly in the range $-0.4 < M/M_s < 0.4$.

To evaluate the influence of the geometry on the wall profile, the dimensions of the constriction have been varied systematically. Figure 3 presents the evolution of w^* as a function of d_0 and S_0 for magnetic elements of constant dimensions, $10 \mu\text{m} \times 4 \mu\text{m} \times 7.5 \text{ nm}$. For $S_0 = 500 \text{ nm}$ and $d_0 < 100 \text{ nm}$, the average DW width is almost constant. However, a steep increase of w^* occurs as d_0 becomes larger than 100 nm . A similar variation is observed when $S_0 = 250 \text{ nm}$, but the increase of w^* at large d_0 values is steeper. Finally, a clear reduction of the wall width is found for even smaller constrictions with $S_0 = 100 \text{ nm}$ and $d_0 < 100 \text{ nm}$. The numerical simu-

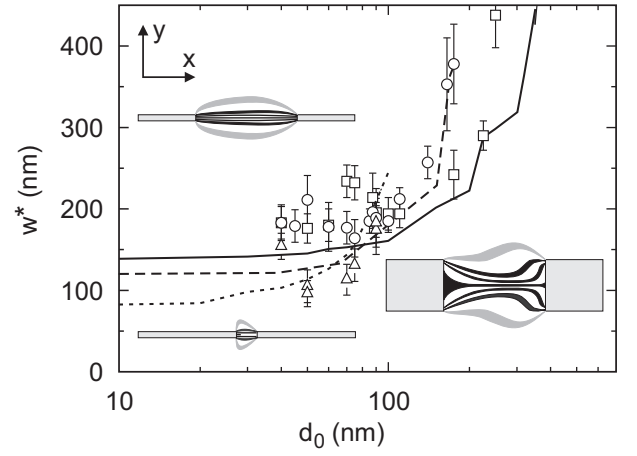


FIG. 3: Evolution of the average DW width w^* vs. constriction dimension d_0 in $\text{Fe}_{20}\text{Ni}_{80}$ with S_0 as parameter ranging from 100 nm (triangles, dotted line) to 250 nm (circles, dashed line) and 500 nm (squares, solid line); element size: $10 \mu\text{m} \times 4 \mu\text{m} \times 7.5 \text{ nm}$. Dots are experimental values and lines the calculated DW width. Insets show constant levels of calculated domain configurations. $M_x = 0, 0.25, 0.5M_s$ correspond to the core of the domain wall (black) and $M_x = 0.75M_s$ to its tails (grey). $d_0 = 30 \text{ nm}$ and $S_0 = 100 \text{ nm}$ (lower left), $d_0 = 30 \text{ nm}$ and $S_0 = 1 \mu\text{m}$ (upper left), $d_0 = 225 \text{ nm}$ and $S_0 = 500 \text{ nm}$ (right).

lations reproduce the experimental trend well and allow us to explain the observed wall-width variations qualitatively.

Consider an unconstrained 180° Néel wall in an extended film. Its total energy is given by the wall energy density multiplied by the total length. The wall width results from the minimization of the energy density, and is solely determined by the material parameters. A DW located in a constriction, however, is affected by the constriction geometry. At the constriction edges, the magnetization is forced to lie parallel to the sides to minimize the surface dipolar energy, and hence the wall width locally corresponds to d_0 . To minimize its total energy in such a geometry, the DW deforms in the constriction area, i.e., the local wall width depends on the distance from the constriction center, and the wall adopts a two-dimensional shape. We consider the two limiting cases of small and large d_0 . The relevant length scale to compare with is the wall width without constriction, w_0 , which deviates from the wall width in an extended film as discussed below.

For $2d_0 < w_0$, an outward deformation of the DW results (see insets on the left in Fig. 3). For large S_0 , this deformation is restricted to the edge region and does not affect the DW profile in the center of the constriction. The measured average width is then almost constant and $w^* \simeq w_0$. For smaller S_0 , however, the center wall width cannot be kept at w_0 . It costs too much exchange energy to let the local wall width vary rapidly along the constriction. Therefore, the wall at the center reduces its width to less than w_0 . Accordingly, below a threshold

value of $S_0 \simeq 250$ nm, a reduction of w^* is observed with decreasing S_0 , which becomes most pronounced for small S_0 .

For $2d_0 > w_0 \simeq 200$ nm, the wall width at the constriction edges expands and the wall deforms inward (see inset on the right in Fig. 3). The same energy arguments as above apply: For small S_0 , the wall at the center stretches, resulting in an increase of the measured w^* . The larger S_0 the stronger the confinement of the wall deformation to the edge region, and consequently the increase of w^* is postponed to larger d_0 values.

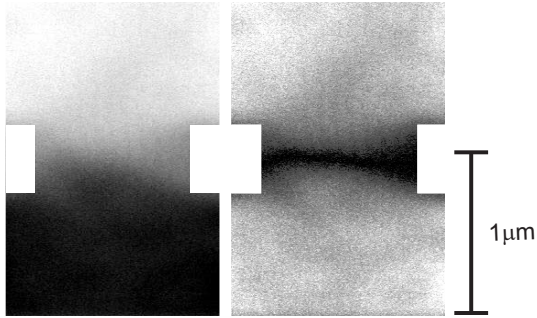


FIG. 4: DW configuration measured in a constriction with $d_0 = 225$ nm and $S_0 = 500$ nm; element size: $10 \mu\text{m} \times 4 \mu\text{m} \times 7.5$ nm. Grey-scale images correspond to the magnetization component parallel (left) and perpendicular (right) to the wall. The wall is asymmetric with respect to the left and right constriction edges. The position of the constriction has been determined from the topographic image.

Figure 4 illustrates the complexity of the DW in the constriction. The wall is two-dimensional and asymmetric, in good agreement with the calculated configuration. In the constriction region, the magnetization has to undergo a 180° rotation. As exchange forces the spins to remain as closely aligned with each other as possible, the 180° turn happens over a larger distance in the outer part of the turn. This explains the asymmetry of the DW configuration. We emphasize that the complex two-dimensional structure of a DW is not restricted to the Néel wall. We have also simulated Bloch walls and find similar features: bent walls and complex two-dimensional patterns. The assumption that a Bloch wall can be treated as a one-dimensional object¹ is only justified for $d_0 \ll S_0$. Otherwise, dipolar contributions force the Bloch wall configuration to adopt a Néel-type arrangement.

Figure 4 also reveals the presence of a small intermediate domain nucleated at one constriction edge. This results from a strong preference for low-angle DWs in the case of Néel walls: Energy can be gained by replacing the 180° domain wall by two 90° walls and an intermediate domain. The splitting into two 90° walls is local at first and will not affect the average DW profile significantly. But as d_0 approaches S_0 , this domain expands to the constriction center, leading to the complete separation of the 180° wall into two 90° walls. This is experimentally visible in the average wall profile, as shown in Fig. 5 for

a constriction of dimensions $S_0 = d_0 = 250$ nm. Thus, an additional condition needs to be fulfilled to avoid wall splitting and to pin a narrower 180° DW in a constriction. Apart from S_0 being small, also $d_0 < S_0$ is required.

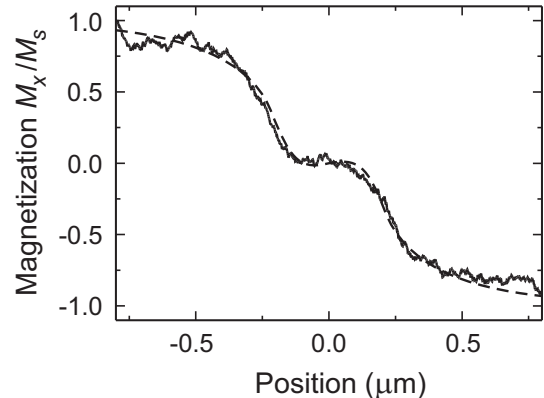


FIG. 5: Wall profile determined in a wide constriction with $S_0 = 250$ nm and $d_0 = 250$ nm showing the splitting of the wall into two individual 90° walls. Experimental data are shown as a solid line, the simulation as a dashed line; element dimensions: $10 \mu\text{m} \times 4 \mu\text{m} \times 7.5$ nm.

Having considered the effect of the constriction dimensions on the DW width, let us discuss the influence of the element size. In an infinitely extended 10-nm-thick $\text{Fe}_{20}\text{Ni}_{80}$ film, the Néel wall width has been determined to be on the order of 100 nm,^{21,22} with tails extending several micrometers beyond the core. In our small magnetic element, however, the tails are limited by the element width $2d_1$, leading to modified profile and wall width. Compared with the unconstrained extended film, the magnetostatic charges need to be redistributed within the Néel wall. This rearrangement of charges is rather complex and has not yet been described theoretically.²³ Figure 6 shows the variation of the wall width w_0 determined for rectangular elements of varying lateral size. Both, our experimental results and micromagnetic simulations demonstrate that a strong reduction of w_0 occurs when decreasing $2d_1$, owing to the confinement of the wall in the micrometer-sized element. Such a dependence on the magnetic-element dimensions is specific of the Néel wall and is not expected to occur for a Bloch wall.

Finally, let us comment on the small discrepancy observed between the experimental and calculated DW widths at small d_0 . This is reminiscent of other experimental DW profile measurements in which the DW width was found to be much larger than the simulated values.¹⁹ It was proposed that the magnetocrystalline anisotropy is smaller and/or the exchange constant larger than assumed in the calculations. Anisotropy can be ruled out in our case. The fact that the discrepancy arises only at small d_0 , at which exchange is predominant, corroborates that exchange might be underestimated in the simulations.

In conclusion, we have investigated the configuration of 180° Néel walls pinned in patterned constrictions, both

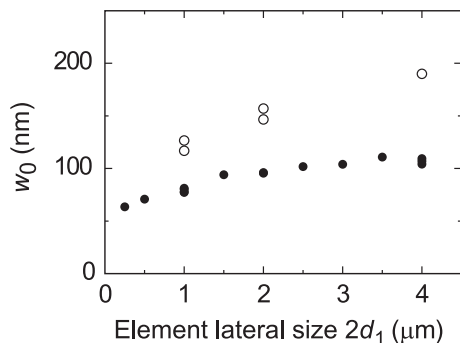


FIG. 6: Evolution of the average DW width w^* as a function of the rectangle's lateral size $2d_1$, with experimental results (empty circles) and calculations (filled circles). While a constriction was needed to pin a 180° Néel wall its dimensions are such that w^* equals w_0 (see Fig. 3): $S_0 = 250$ nm and $d_0 = 50$ nm. The element thickness is 20 nm.

experimentally and by micromagnetic simulations. Isolated domain walls present a complex configuration which is two-dimensional and asymmetric. We have further demonstrated that their average width can be tuned by the dimensions of both the element and the constriction.

Because of the extended tails in the Néel walls, the wall width in micrometer-sized elements can be strongly reduced, compared with the infinitely extended thin film. The width decreases when the lateral size of the magnetic element $2d_1$ decreases. In addition, by tuning the constriction dimensions, the Néel-wall width can also be modified continuously. Owing to significant dipolar contributions at the constriction edges, the domain wall can be stretched to wide profiles for large constriction widths $2d_0$. For small d_0 , on the other hand, the domain wall is strongly confined when the constriction length $2S_0$ decreases. The ability to control domain-wall profile properties through geometrical constraints calls for further investigation of other domain-wall properties such as the magnetoresistance, or the displacement of constrained magnetic domain walls.

We acknowledge James Jarratt and Ian McFadyen for providing us with the $\text{Fe}_{20}\text{Ni}_{80}$ films, Michel Despont, Hugo Rothuizen, Ute Drechsler, and Richard Stutz for their contribution in the patterning processes of the films, and Daniele Mauri and Jerome Wolfman for their input in the initial phase of the project.

* Electronic address: pju@zurich.ibm.com

- ¹ P. Bruno, Phys. Rev. Lett. **83**, 2425 (1999).
- ² O. Pietzsch, A. Kubetzka, M. Bode, and R. Wiesendanger, Phys. Rev. Lett. **84**, 5212 (2000).
- ³ N. Garcia, M. Muñoz, and Y.-W. Zhao, Phys. Rev. Lett. **82**, 2923 (1999).
- ⁴ H. D. Chopra and S. Z. Hua, Phys. Rev. B **66**, 020403(R) (2002).
- ⁵ C. Rüster, T. Borzenko, C. Gould, G. Schmidt, L. W. Molenkamp, X. Liu, T. J. Wojtowicz, J. K. Furdyna, Z. G. Yu, and M. E. Flatté, Phys. Rev. Lett. **91**, 216602 (2003).
- ⁶ D. A. Allwood, G. Xiong, M. D. Cooke, C. C. Faulkner, D. Atkinson, N. Vernier, and R. P. Cowburn, Science **296**, 2003 (2002).
- ⁷ T. Ono, H. Miyajima, K. Shigeto, K. Mibu, N. Hosoi, and T. Shinjo, Science **284**, 468 (1999).
- ⁸ L. Gan, S. H. Chung, K. H. Aschenbach, M. Dreyer, and R. D. Gomez, IEEE Transactions on Magnetics **36**, 3047 (2000).
- ⁹ J. Grollier, D. Lacour, V. Cros, A. Hamzic, A. Vaurs, A. Fert, D. Adam, and G. Faini, J. Appl. Phys. **92**, 4825 (2002).
- ¹⁰ J. Grollier, B. Poulenc, V. Cros, A. Hamzic, A. Vaurs, A. Fert, and G. Faini, Appl. Phys. Lett. **83**, 509 (2003).
- ¹¹ N. Vernier, D. A. Allwood, D. Atkinson, M. D. Cooke, and

- R. P. Cowburn, EuroPhys. Lett. **65**, 526 (2004).
- ¹² A. Yamaguchi, T. Ono, S. Nasu, K. Miyake, K. Mibu, and T. Shinjo, Phys. Rev. Lett. **92**, 077205 (2004).
- ¹³ K. Koike and K. Hayakawa, J. Appl. Phys. **23**, L187 (1984).
- ¹⁴ M. R. Scheinfein, J. Unguris, M. H. Kelly, D. Pierce, and R. J. Celotta, Rev. Sci. Instrum. **61**, 2501 (1990).
- ¹⁵ M. Donahue and D. Porter, <http://math.nist.gov/oommf/>.
- ¹⁶ R. Allenspach, J. Magn. Magn. Mater. **129**, 160 (1994).
- ¹⁷ M. R. Scheinfein, J. Unguris, J. L. Blue, K. J. Coakley, D. Pierce, R. J. Celotta, and P. J. Ryan, Phys. Rev. B **43**, 3395 (1991).
- ¹⁸ A. Berger and H. P. Oepen, Phys. Rev. B **45**, 12596 (1992).
- ¹⁹ C. A. F. Vaz, L. Lopez-Diaz, M. Klaui, J. A. C. Bland, T. L. Monchesky, J. Ungaris, and Z. Cui, Phys. Rev. B **67**, 140405(R) (2003).
- ²⁰ T. VanZandt, R. Browning, and M. Landolt, J. Appl. Phys. **69**, 1564 (1991).
- ²¹ T. Suzuki, C. H. Wilts, and C. E. Patton, J. Appl. Phys. **39**, 1983 (1968).
- ²² B. Y. Wong and D. E. Laughlin, J. Appl. Phys. **79**, 6455 (1996).
- ²³ A. Holz and A. Hubert, Z. angew. Phys. **26**, 145 (1969).